Class IIa HDACs inhibit cell death pathways and protect muscle integrity in response to lipotoxicity

Sheree D. Martin[1,9], Timothy Connor[1,9], Andrew Sanigorski[1], Kevin A. McEwen[1], Darren C. Henstridge[2,3], Brunda Nijagal[4], David De Souza[4], Dedreia L. Tull[4], Peter J. Meikle[3], Greg M. Kowalski[1,5], Clinton R. Bruce[5], Paul Gregorevic[6], Mark A. Febbraio[7], Fiona M. Collier[8], Ken R. Walder[1], Sean L. McGee[1,10]

[1]Institute for Mental and Physical Heath and Clinical Translation (IMPACT) and Metabolic Research Unit, School of Medicine, Deakin University, Geelong, Victoria 3216, Australia;
[2]College of Health and Medicine, School of Health Sciences, University of Tasmania, Launceston, Australia;
[3]Baker Heart and Diabetes Institute, Melbourne, Victoria 3004, Australia;
[4]Metabolomics Australia, The University of Melbourne, Parkville, Victoria 3010, Australia;
[5]Institute of Physical Activity and Nutrition (IPAN) and School of Exercise and Nutrition Sciences, Deakin University, Geelong, Victoria 3216, Australia;
[6]Centre for Muscle Research, Department of Anatomy and Physiology, The University of Melbourne, Parkville, VIC, Australia.
[7]Monash Institute of Pharmaceutical Sciences, Monash University, Parkville, VIC, Australia.
[8]Barwon Health, Geelong, Victoria 3220, Australia
[9]These authors contributed equally to this work
[10]Lead contact

Lead contact:

Professor Sean L. McGee
Metabolic Remodelling Laboratory
Metabolic Research Unit
School of Medicine
Deakin University, Waurn Ponds, Australia, 3216
Ph: +61 3 5227 2519
Fax: +61 3 5227 2945
Email: sean.mcgee@deakin.edu.au

ABSTRACT

Lipotoxicity, the accumulation of lipids in non-adipose tissues, alters the metabolic transcriptome and mitochondrial metabolism in skeletal muscle. The mechanisms involved remain poorly understood. Here we show that lipotoxicity increased histone deacetylase 4 (HDAC4) and histone deacetylase 5 (HDAC5), which reduced the expression of metabolic genes and oxidative metabolism in skeletal muscle. This metabolic reprogramming was linked with reduced expression of p53 pathway genes that mediate apoptosis and ferroptosis, as well as preserved muscle cell viability in response to lipotoxicity. Mechanistically, increased HDAC4 and 5 decreased acetylation of p53 at K120, a modification required for transcriptional activation of apoptosis, while metabolically sensitive redox drivers of ferroptosis were also reduced. Overexpression of loss-of-function HDAC4 and HDAC5 mutants in skeletal muscle of obese *db/db* mice enhanced oxidative capacity, increased apoptosis and ferroptosis and reduced muscle mass. This study identifies HDAC4 and HDAC5 as repressors of the oxidative state of skeletal muscle, which is linked to inhibition of cell death pathways and preservation of muscle integrity in response to lipotoxicity.

INTRODUCTION

Obesity is driving an epidemic of chronic disease, including type 2 diabetes. Linked to these diseases are adverse cellular responses arising from the accumulation of lipids in non-adipose tissues, a process termed lipotoxicity (1). The deleterious effects of lipotoxicity include altered cellular signalling, metabolic reprogramming and cell death (2). Tissues that are particularly susceptible to lipotoxicity include the liver, kidneys, pancreas, heart and skeletal muscle (2).

Lipotoxicity alters skeletal muscle metabolism, inducing insulin resistance and impairments in aspects of oxidative metabolism. Reduced rates of both glucose and lipid oxidation have been observed in the skeletal muscle of obese subjects (3; 4) and data describing impairments in amino acid metabolism are also emerging (5-7). Experimental induction of acute lipotoxicity in humans through lipid infusion results in many of the same skeletal muscle metabolic alterations (8; 9). These impairments in oxidative metabolism are associated with reduced expression of a metabolic and mitochondrial transcriptional program controlled by the peroxisome proliferator-activated receptor-gamma coactivator 1 alpha (PGC-1α) transcriptional coactivator (10), encoded by the *PPARGC1A gene*. It is not known why repression of the metabolic transcriptome and reduced oxidative metabolism is an adaptation to lipotoxicity and the molecular pathways involved remain unclear.

Studies from our group and others have found that the class IIa histone deacetylase (HDAC) isoforms 4 and 5 are regulators of PGC-1α expression in skeletal muscle (11; 12). HDAC4 and 5 act co-operatively as heterodimers to repress the myocyte-enhancer factor 2 (MEF2) family of transcription factors (13; 14). Repression of MEF2 transcriptional activity by the class IIa

HDACs is prevented by their phosphorylation-dependent nuclear export (15). HDAC4 and 5 are sensitive to energetic stress, such as during exercise, through phosphorylation by the AMP-activated protein kinase (AMPK) (16-18), which in turn activates transcriptional programs that enhance oxidative metabolism and capacity, including expression of PGC-1α and its transcriptional programs (11; 18; 19). Binding sites for the MEF2 transcription factor are found in the *PPARGC1A* promoter (12) and in the promoters and enhancer regions of other genes involved in oxidative metabolism (11). These findings suggest that the class IIa HDACs are a hub regulating skeletal muscle metabolic transcriptional programs in response to changes in energy balance. However, the role of the class IIa HDAC transcriptional repressors in the context of lipotoxicity is unknown. The current study sought to determine whether HDAC4 and 5 contribute to the suppression of metabolic genes and oxidative metabolism in response to lipotoxicity and to understand why these adaptations occur.

METHODS

Cell culture

Mouse C2C12 myoblasts and myotubes were cultured using standard methods. Cells stably overexpressing HDAC4 and 5 were analysed as myoblasts as HDAC4 and 5 prevented myogenic differentiation of these cells to myotubes. Treatment doses of palmitate (Sigma-Aldrich), camptothecin (Sigma), Erastin (Sigma), 1S,3R-RSL 3 (Sigma) and Ferrostatin (Selleckchem) are reported in Figure legends and were applied for 24h unless otherwise stated. Palmitate was dissolved in ethanol at 70°C and diluted in ultrapure H_2O before conjugation to fatty acid-free BSA at 1:10 ratio (w/v). An ethanol and BSA solution without palmitate was prepared at the same time for use as a vehicle and stored at -20°C.

Animal models

All animal experimentation was approved by the Deakin University Animal Ethics Committee (G27-2012 and G21-2015). Mice were acquired from the Animal Resources Centre (Perth, WA, Australia) and were group housed with a 12hr light/dark cycle, temperature 21± 3°C, humidity 30-70%. Animals had *ad libitum* access to standard rodent chow and water. Heterozygous C57BL/6J *db/+* and homozygous *db/db* mice were fasted for 5 hr prior to humane killing by cervical dislocation for rapid excision of tissues, which were snap frozen in liquid nitrogen. C57BL/6J mice were administered recombinant serotype 6 adeno-associated viral (AAV6) (rAAV6) vectors via intramuscular injection into the anterior and posterior compartments of the lower hind limbs. Each compartment of the left limb received $2e^{10}$ vector genomes (vg) of empty rAAV6, whilst each compartment of the right limb received $1e^{10}$ vg of WT HDAC4 rAAV6 and $1e^{10}$ vg of WT HDAC5 rAAV6. *db/db* mice were similarly administered rAAV6 vectors via intramuscular injection. Each compartment of the left limb received $5e^{10}$ vg of

empty rAAV6, whilst each compartment of the right limb received $2.5e^{10}$ vg of DN HDAC4 rAAV6 and $2.5e^{10}$ vg of DN HDAC5 rAAV6. Experiments were performed ~8 weeks after rAAV6 administration. At the conclusion of experiments mice were fasted for 4 hours before humane killing by cervical dislocation. Tissues were rapidly excised and snap frozen in liquid nitrogen or fixed in 10% formalin.

Respiration and mitochondrial function analysis

Mitochondrial function in cells were treated with vehicle (BSA) or palmitate was assessed as previously described (20) and respiratory analysis of skeletal muscle biopsies was also performed as previously described (11).

Lipidomics and metabolite analysis

To determine cellular lipid profiles, ~$1e^6$ cells were collected in 100µl of PBS and frozen at -80°C, or ~10mg of muscle was homogenised in 100µl of PBS, and lipids were determined as previously described (21). For detection of Glu and GSH, cells in 6-well plates underwent metabolic arrest by washing in 1mL ultrapure water before being frozen instantaneously by the addition of liquid nitrogen. To extract polar metabolites, ice-cold methanol:chloroform (9:1) containing internal standards (0.5nM 13C-sorbitol and 5nM 13C, 15N-valine) was added. Metabolites were detected using LC and high resolution QTOF mass spectrometry previously described(22) with the following modifications. Samples (10µL) were injected onto an Agilent 1290 LC fitted with a SeQuant ZIC®-pHILIC column (2.1 x 150 mm, 5µm; Merck) using 20mM ammonium carbonate, pH 9.0 (Sigma-Aldrich) and 100% acetonitrile as the mobile phases.

Microarray and gene expression analysis

For comparative transcriptomics analysis, each group consisted of three biological replicates and microarray analysis was performed as previously described (11). Genes found to be significantly altered in the same direction in both cell and skeletal muscle data sets (n = 236) were analysed by gene set enrichment analysis from all KEGG pathway lists. The microarray datasets generated conforms to MIAME guidelines and is available at Gene Expression Omnibus (GSE215185). Gene expression was measured using real time RT-PCR as previously described (18). Primer sequences are available in Table S1.

Immunoprecipitation and western blot analysis

Cells were collected in lysis buffer (50mM Tris pH 7.5, 1mM EDTA, 1mM EGTA, 10% glycerol, 1% Triton X-100, 50mM NaF, 5mM sodium pyrophosphate, 1mM DTT, 1X protease inhibitor cocktail (Sigma)) and ~20mg skeletal muscle was homogenised in 10 volumes of lysis buffer using a handheld homogeniser. Protein concentration was determined using the BCA assay (Pierce). Immunoprecipitation and western blotting were performed as previously described (23). Antibody details are listed in Table S2.

Insulin/isotopic glucose administration and stable isotope metabolomics

Mice were administered 200uCi/kg of 2[1,2-^{3}H]-deoxyglucose and 100uCi/kg of 1-^{14}C glucose, with or without 1.2U/kg insulin, following a 5hr fast. Blood glucose was determined using a handheld glucometer (Accu-Chek Performa, Roche) and ~5µL blood was obtained from the tail tip prior to tracer administration and 5, 15 and 30min after tracer administration. Plasma tracer concentration and tissue 2-deoxyglucose clearance were determined as we have previously described (24). To determine 1-^{14}C glucose incorporation into glycogen, ~10-15mg

of TA muscle was digested in 1M KOH at 70°C for 20 min and glycogen was precipitated with saturated Na_2SO_4, washed twice with 95% ethanol and resuspended in acetate buffer (0.84% sodium acetate, 0.46% acetic acid, pH 4.75) containing 0.3mg/mL amyloglucosidase (Sigma). Glycogen was digested overnight at 37°C before glucose content was quantified using the glucose oxidase method (20) and ^{14}C-glucose incorporation was measured. To determine 1-^{14}C glucose incorporation into lipids, 5-10mg of TA muscle was homogenised in chloroform/methanol (2:1) and mixed overnight at room temperature. Organic and inorganic phases were separated, and the lower organic phase was collected and evaporated under N_2 at 45°C. The dried extract was resuspended in absolute ethanol and TG content was assayed using TG GPO-PAP reagent (Roche) and ^{14}C-glucose incorporation was measured.

To assess oxidative glucose utilisation, mice were administered a bolus of 50mg of [U-^{13}C] glucose (Sigma-Aldrich) via oral gavage. At 60 min later, mice were humanely killed by cervical dislocation and skeletal muscles were immediately collected. Targeted metabolomics and analysis of [U-^{13}C] labelling was performed as we have previously described (24). Total labelling in HDAC4 and 5 over expressing muscle was expressed relative to labelling in the corresponding control muscle within each mouse.

Measurement of apoptosis and cell viability.

Analysis of apoptotic cells was performed by dual staining with FITC-conjugated Annexin V (BD Pharmingen) and propidium iodide (PI; Molecular Probes) and was optimised for adherent cells. For measurement of apoptosis in tissues, caspase 3 activity was measured using Caspase-Glo 3/7 assay (Promega). Quantification of viable cells was performed by

staining with 7-aminoactinomycin D (7-AAD; BD Pharmingen) and flow cytometry or with crystal violet staining with colorimetric detection.

Reactive oxygen species detection

In cells, hydrogen peroxide (H_2O_2) was detected using Amplex Red assay (Invitrogen). Cells were seeded into a 96-well plate at 25,000 cells/well. The following day, cells were treated with vehicle (DMSO), 100µM mitoTEMPO or 100µM apocynin for 30 min at 37°C. Cells were then co-incubated with 50µM Amplex Red and 0.1U/ml horseradish peroxidase (HRP) for a further 30 min at 37°C. Mitochondrial ROS was designated as that sensitive to MitoTEMPO, while NADPH oxidase ROS was designated as that sensitive to apocynin. For tissues, the OxiSelect In Vitro ROS/RNS Assay kit (Green Fluorescence) (Cell Biolabs Inc.) was used according to the manufacturer's instructions.

GPX4 activity and lipid peroxidation

Glutathione dependent peroxidase activity was measured using a colorimetric Glutathione Peroxidase Assay Kit (AbCam). Cells were plated into 10cm tissue culture plates at $4x10^6$ cells per dish. After 3hrs, media was refreshed and cells incubated for 1hr, washed and collected in 250ul of supplied assay buffer. For tissues, muscle lysate was analysed. Data was then analysed as described by the manufacturer with results normalized to protein concentration. Lipid peroxidation in both cells and muscle lysates was assessed using a lipid peroxidation kit (Sigma). The assay was performed according to manufacturer's instructions, including addition of butanol to the reaction.

Histology

Fixed TA muscles were embedded in paraffin before transverse sections were obtained at 5μm thickness and stained for H&E and Masson's trichrome. Slides were scanned (Aperio, Leica Biosystems) and were analysed using photoshop and image J to quantify fibre diameter and cell number.

Statistical analysis.

All data are expressed as mean ± SEM. Individual data points identified as greater than two standard deviations away from the mean were designated as outliers and removed from the dataset. Data was assessed for normality using the Shapiro-Wilk test. Differences between groups were assessed using t-test, Kruskal-Wallis test, one-way ANOVA or two-way ANOVA as appropriate using GraphPad Prism. Specific differences between groups were identified using Dunn's or Tukey's multiple comparisons tests. For animal experiments where opposing hind limbs were administered different rAAVs, such that control and experimental conditions were contained within the one animal, paired t-tests were used. Differences were considered statistically significant where $p<0.05$.

RESULTS

HDAC4 and 5 are increased in models of lipotoxicity

To test the hypothesis that HDAC4 and 5 are increased by lipotoxicity, C2C12 myotubes were exposed to 0.25 or 0.5mM palmitate, or BSA (vehicle), for 16 hr. Lipidomic profiling indicated ceramide and DG species were increased following exposure to 0.5mM palmitate, while increases in some TG species were observed following exposure to both 0.25mM and 0.5mM palmitate (Figure 1A). Total Cer levels were increased by both 0.25mM and 0.5mM palmitate while total DG and TG levels were increased by 0.5mM palmitate (Figure 1B). Consistent with the known effect of palmitate on C2C12 cells, application of 0.25mM and 0.5mM palmitate was associated with lower *Ppargc1a* gene expression (Fig. 1C) and a significant reduction in cellular respiration (Fig. 1D). The abundance of HDAC5 protein was increased by both 0.25 and 0.5mM palmitate, while HDAC4 protein abundance was increased by 0.5mM palmitate (Figure 1E). There were no differences in *Hdac4* or *Hdac5* gene expression between groups (Supplementary Fig. 1A).

To examine these mechanisms *in vivo*, the tibialis anterior skeletal muscle of obese *db/db* and control heterozygous littermate mice was analysed. Specific ceramide, DG and TG species (Fig. 1F) and total ceramides and DG were increased in skeletal muscle of *db/db* mice (Fig. 1G). The increased muscle lipid concentrations in these obese mice were associated with decreased *Ppargc-1*α gene expression (Fig. 1H), reduced respiratory responses in skeletal muscle biopsies (Fig. 1I) and increased HDAC4 and 5 protein abundance (Fig. 1J). Skeletal muscle gene expression levels of *Hdac5*, but not *Hdac4*, were increased in *db/db* mice

(Supplementary Fig. 1B). Notwithstanding the complex physiology of the *db/db* model, these data suggest that skeletal muscle HDAC4 and 5 are increased in response to lipotoxicity and are associated with reduced *Ppargc1a* expression and impaired oxidative metabolism.

Overexpression of HDAC4 and 5 in skeletal muscle represses *Pppargc1a* expression and oxidative capacity

To examine whether increased HDAC4 and 5 impacts skeletal muscle metabolism, a bilateral skeletal muscle HDAC4 and 5 mouse model was developed using rAAV6 vectors expressing HDAC4 and HDAC5 (Fig. 2A). Administration of HDAC4 and 5 rAAV6 vectors increased *Hdac4* and *Hdac5* gene expression (Fig. 2B) and protein (Fig. 2C) in tibialis anterior (TA) muscle. Overexpression of HDAC4 and 5 reduced *Ppargc1a* expression (Fig. 2D) and reduced the expression of a range of MEF2 and PGC-1α target genes involved in oxidative and mitochondrial metabolism (Fig. 2E). These changes in metabolic transcripts were associated with reduced abundance of ATP synthase subunits, but not other subunits of electron transport chain complexes (Fig. 2F). Reduced ATP synthase components was associated with an overall main effect for respiratory responses to be reduced in biopsies of muscles overexpressing HDAC4 and 5 when driven by both succinate (Fig. 2G) and malate (Fig. 2H) as substrates. Overexpression of HDAC4 and 5 was not associated with lipid accumulation, although all lipid species tended to be higher in skeletal muscle overexpressing HDAC4 and 5 (Fig. 2I). These data indicate that increasing HDAC4 and 5 represses *Ppargc1a* gene expression and oxidative capacity in skeletal muscle.

Overexpression of HDAC4 and 5 in skeletal muscle inhibits oxidative glucose utilisation

Reduced skeletal muscle oxidative capacity that is associated with lipotoxicity has been linked with reduced insulin action and impaired glucose utilisation (4; 25; 26). The impact of HDAC4 and 5 overexpression on glucose metabolism was examined. In bilateral skeletal muscle HDAC4 and 5 mice administered vehicle or insulin (1.2U/kg i.p.) with ^{3}H-2-deoxyglucose (2-DG) and ^{14}C-glucose tracers (Fig. 3A), insulin reduced the excursion of both tracers (Supplementary Fig. 3A and B). There was a main effect for increased glucose clearance by skeletal muscles overexpressing HDAC4 and 5 (Fig. 3B). When expressed relative to control skeletal muscle within each mouse, HDAC4 and 5 overexpression increased glucose clearance in vehicle but not insulin-stimulated conditions (Fig. 3C). Overexpression of HDAC4 and 5 increased glucose incorporation into glycogen (Fig. 3D) and increased glycogen concentration (Supplementary Fig. 3C). In contrast there was a main effect for insulin to increase glucose incorporation into lipids (Fig. 3E), which was associated with main effects for insulin to increase Akt phosphorylation at T308 (Fig. 3G) and S473 (Fig. 3H). However, consistent with the glucose clearance data, there was a main effect for increased phosphorylation of TBC1D4 at S642 in skeletal muscles overexpressing HDAC4 and 5 (Fig. 3I). These data suggest that overexpression of HDAC4 and 5 increased non-oxidative glucose utilisation in skeletal muscle.

To further examine the effect of HDAC4 and 5 overexpression on oxidative glucose utilisation, a targeted stable isotope metabolomics approach following an oral bolus of U^{13}C-glucose was used in bilateral skeletal muscle HDAC4 and 5 mice (27) (Fig. 3J). Overexpression of HDAC4 and 5 increased the abundance of lactate and succinate (Fig. 3K) and total ^{13}C labelling of succinate and malate (Fig. 3L). Isotopologue analysis revealed accumulation of both M+0 and

M+2 lactate in muscle overexpressing HDAC4 and 5 (Fig. 3M), suggesting both increased non-oxidative glucose utilisation and increased malate/pyruvate cycle flux, respectively (28). Succinate M+0, M+1 and M+2 isotopologues were increased in muscle overexpressing HDAC4 and 5 (Fig. 3N), consistent with a major impairment in SDH activity (29), which is bifunctional for both the TCA cycle and the electron transport chain. These data are also supported by reduced succinate-driven respiration in muscles overexpressing HDAC4 and 5 (Fig. 2G). Similarly, HDAC4 and 5 overexpression was associated with increased malate M+0 and M+1 isotopologues (Fig. 3O). Together, these data indicate that increased HDAC4 and 5 is linked with defective oxidative utilisation of glucose in skeletal muscle.

HDAC4 and 5 enhance cell survival in response to lipotoxicity and supress the apoptosis and ferroptosis cell death pathways

Overexpression of HDAC4 and 5 impaired mitochondrial function and reprogrammed glucose metabolism, increasing non-oxidative glucose utilisation and inhibiting oxidative glucose utilisation. To better understand why this metabolic reprogramming occurs, important genes regulated by HDAC4 and 5 in the context of lipotoxicity were identified using a comparative transcriptomics approach. Specifically, the transcriptome altered in the skeletal muscle of *db/db* mice in which HDAC4 and 5 was increased (Fig. 1J) was compared to the transcriptome altered in myogenic C2C12 myoblasts stably overexpressing HDAC4 and 5 (Supplementary Fig. 4A). Overexpression of HDAC4 and 5 in these cells reduced *Ppargc1a* gene expression, suppressed OXPHOS and TCA cycle genes, and reduced oxidative capacity (Supplementary Fig. 4B-D). The comparative transcriptomic analysis and subsequent pathway analysis of

coregulated genes revealed the p53 signalling pathway related to cell survival as the only significantly regulated pathway (Supplementary Fig. 4E).

Profiling of genes downstream of p53 in this pathway in C2C12 myoblasts overexpressing HDAC4 and 5 revealed that several pro-apoptosis genes were reduced, including *Casp3* and *9, Cycs, Pmaip1* and *Bbc3* (Fig. 4A), consistent with suppression of apoptosis. Similarly, genes involved in ferroptosis, a form of iron-mediated cell death involving lipid peroxidation (30), were altered in ways that indicated suppression of ferroptosis, including increased *Slc7a11* expression and reduced *Sat1* and *Alox15* expression (Fig. 4A). These data suggest that increased HDAC4 and 5 inhibit apoptotic and ferroptotic cell death pathways. Indeed, overexpression of HDAC4 and 5 in C2C12 myoblasts reduced the number of apoptotic cells following exposure to the apoptosis-inducing agent camptothecin (Fig. 4B). Similarly, viability was higher in cells overexpressing HDAC4 and 5 following exposure to the ferroptosis-inducing agent RSL3 (Fig. 4C). These data raised the possibility that HDAC4 and 5 suppress the apoptosis and ferroptosis pathways to enhance cell survival in response to lipotoxicity. To test this hypothesis, cells were exposed to increasing concentrations of palmitate intended to challenge cell voiability. Overexpression of HDAC4 and 5 enhanced the viability of cells exposed to both 1 and 2mM of palmitate compared with control cells and resulted in cells being largely resistant to lipotoxicity (Fig. 4D). This protection of cell viability was associated with reduced cleavage of caspase 3 and 9, the irreversible events that trigger apoptosis (Fig. 4E), as well as fewer apoptotic cells (Fig. 4F) in response to increasing concentrations of palmitate. Overexposure of western blots showed that endogenous HDAC4 and 5 were increased by these high concentrations of palmitate (Supplementary Fig. 4F), similar to the lower concentrations of palmitate characterised previously (Fig. 1E). Similarly, overexpression

of HDAC4 and 5 reduced lipid peroxidation, the trigger for ferroptosis induced-cell death, in response to increasing concentrations of palmitate (Fig. 4H). These data indicate that increased HDAC4 and 5 inhibit the apoptosis and ferroptosis cell death pathways and enhance cell viability in response to lipotoxicity.

HDAC4 and 5 inhibit apoptosis by reducing p53 K120 acetylation

In several cancer cell types, HDAC5 has been linked with reduced acetylation of p53 at K120, which inhibits p53 transcriptional activity and the expression of apoptosis genes, which reduces apoptosis sensitivity (31-33). Furthermore, acetylation of p53, including at K120, can contribute to the transcriptional regulation of ferroptosis (34). To explore whether reduced acetylation of p53 at K120 is involved in suppression of apoptosis and ferroptosis by HDAC4 and 5 in myogenic cells, C2C12 myoblasts stably overexpressing HDAC4 and 5 were transfected with wild type p53, or p53 in which K120 was mutated to either glutamine (K120Q; acetylation mimetic gain-of function) or arginine (K120R; deacetylation mimetic loss-of-function) (Fig. 5A). The acetylation of p53 at K120 was reduced by the overexpression of HDAC4 and 5 (Fig. 5A). In cells overexpressing HDAC4 and 5, introduction of the $p53^{K120Q}$ acetylation mimetic mutant restored the expression of the pro-apoptosis genes *Casp3, Casp9* and *Cycs* (Fig. 5B). However, the expression of *Slc7a11*, which opposes ferroptosis, was not influenced by expression of this mutant (Fig. 5B). This suggests that reduced acetylation of p53 at K120 by HDAC4 and 5 suppresses apoptosis, but not ferroptosis, transcriptional programs. Expression of $p53^{K120Q}$ also restored apoptosis in HDAC4 and 5 overexpressing cells exposed to the apoptosis-inducing agent camptothecin (Fig. 5C). Although p53 is also known to regulate aspects of cellular metabolism(35), gain and loss-of-function K120 p53 mutants

had no effect on either oxidative (Supplementary Fig. 5A) or glycolytic flux (Supplementary Fig. 5B). To determine whether p53 K120 acetylation determines cell viability in response to lipotoxicity, cells expressing WT p53 or $p53^{K120R}$ were exposed to 2mM palmitate. However, the $p53^{K120R}$ mutant did not influence cell viability in response to palmitate exposure (Fig. 5D). Furthermore, the apoptosis inhibitor, Z-DED-FMK, had no effect on cell viability in response to palmitate exposure (Fig. 5E), suggesting that other mechanisms are also involved in the cell death response to lipotoxicity.

HDAC4 and 5 inhibit multiple metabolic inputs to the ferroptosis pathway

As suppression of apoptosis through reduced p53 acetylation alone was not sufficient to explain the protective effect of HDAC4 and 5 on cell survival in response to lipotoxicity, the role of ferroptosis-mediated mechanisms of cell death (Fig. 5F) were further explored. The ferroptosis inhibitor Ferrostatin enhanced C2C12 myoblast viability following exposure to 2mM palmitate (Fig. 5G). Overexpression of HDAC4 and 5 enhanced cell viability in response to increasing concentrations of Erastin (Fig. 5H), an agent that induces ferroptosis by inhibiting system x_c and glutamate and cysteine exchange(36), which in turn reduces glutathione (GSH) levels and results in lipid peroxidation through multiple mechanisms (Fig. 5F). Consistent with HDAC4 and 5 increasing the expression of *Slc7a11* (Fig. 4A), overexpression of HDAC4 and 5 reduced intracellular glutamate concentrations, tended to increase intracellular GSH and increased the GSH/glutamate ratio (Fig. 5I). This was associated with increased glutathione peroxidase (GPX) activity in cells overexpressing HDAC4 and 5 (Fig. 5J) and reduced total H_2O_2 production (Supplementary Fig. 5C), including from mitochondria and NADPH oxidases (Fig. 5K). Together, these data indicate that increased HDAC4 and 5

alters the metabolism-sensitive redox inputs to ferroptosis, consistent with inhibition of this pathway.

Ferroptosis involves peroxidation of polyunsaturated (PU) phosphatidylethanolamine (PE) and phosphatidylcholine (PC) lipids, particularly those with arachidonic acid (AA) or adrenic acid (Ada) fatty acid species (37). Changes in the levels of these lipid species have been linked to alterations in ferroptosis sensitivity (37). In lipidomic data from skeletal muscle bilateral HDAC4 and 5 mice, overexpression of HDAC4 and 5 had no effect on any specific PU-PE or PU-PC species between groups, although most lipid species tended to be higher in muscle overexpressing HDAC4 and 5 (Supplementary Fig. 5D). However, it should be noted that HDAC4 and 5 reduced the gene expression of *Alox15* (Fig. 4A), which catalyses lipid peroxidation (Fig. 5F), and of *Sat1* (Fig. 4A), which is a transcriptional regulator of *Alox15* (38). The extent of lipid saturation has also been linked to lipotoxicity induced cell death (39), however there were no differences in lipid saturation when expressed either as absolute abundance (Supplementary Fig. 5E) or proportion of total lipids (Supplementary Fig. 5F). This suggests that HDAC4 and 5 have minimal effect on the abundance of lipid species but reduces expression of enzymes that mediate lipid peroxidation. Together, these findings indicate that increased HDAC4 and 5 alter cellular redox balance and expression of *Alox15*, which contributes to inhibition of ferroptosis.

HDAC4 and 5 are required to suppress apoptosis and ferroptosis and maintain muscle mass in obese mice

To establish whether HDAC4 and 5 suppress apoptosis and ferroptosis in skeletal muscle in response to lipoxicity *in vivo*, a bilateral skeletal muscle loss-of-function HDAC4 and 5 model was developed in obese *db/db* mice using AAV6 vectors (Fig. 6A). This loss-of-function approach employed active-site HDAC4 and 5 mutants (D832N HDAC4 and D861N HDAC5), which we have previously described as acting in a dominant negative (DN) manner when overexpressed (11). Overexpression of these mutants in skeletal muscle increases the expression of *Ppargc1a* and other metabolic genes and enhance oxidative metabolism(11). Intramuscular administration of AAV6 vectors expressing DN HDAC4 and 5 to *db/db* mice increased HDAC4 and 5 gene (Fig. 6B) and protein (Fig. 6C) expression and increased the expression of *Ppargc1a* (Fig. 6D). Consistent with these findings, there was a main effect for respiratory responses to be increased in muscle biopsies expressing DN HDAC4 and 5 (Fig. 6E). Expression of DN HDAC4 and 5 increased caspase 3 activity (Fig. 6F) and lipid peroxidation (Fig. 6G), functional readouts of apoptosis and ferroptosis, respectively. Examination of the mechanisms involved in HDAC4 and 5-mediated apoptosis revealed that p53 acetylation of K120 tended to be higher (Fig. 6H), and the expression of p53-dependent pro-apoptosis genes, including *Casp3, Casp9* and *Bbc3* was increased (Fig. 6I). The ferroptosis mechanisms regulated by HDAC4 and 5 were also examined. In contrast to observations in myogenic cells, the expression of *Slc7a11* in skeletal muscle was low and close to assay detection limits (Supplementary Fig. 6A). This suggests that system x_c likely has only a minor role in the regulation of ferroptosis in skeletal muscle. There were no differences in GPX activity between groups (Supplementary Fig. 6B). However, expression of DN HDAC4 and 5 increased ROS (Fig.

6J) and increased *Sat1* and *Alox15* expression (Fig. 6K), indicating that increased capacity for lipid peroxidation. Increased apoptosis and ferroptosis in skeletal muscles expressing DN HDAC4 and 5 was associated with reduced mass of the gastrocnemius and the TA muscles (Fig. 6L). In the TA muscle, there was no difference in fibre diameter between groups (Supplementary Fig. 6C). However, Masson's trichrome staining showed sporadic areas of localised fibrosis in response to DN HDAC4 and 5 overexpression (Fig. 6M). In skeletal muscles overexpressing DN HDAC4 and 5 there were also discreet regions of fibres with centralised nuclei (Fig. 6N), which is indicative of regenerating muscle fibres. These data show that HDAC4 and 5 are required to suppress apoptosis and ferroptosis and to maintain muscle mass and integrity in obese mice.

DISCUSSION

Lipotoxicity has a major impact on the metabolism, function and survival of various tissues including skeletal muscle. The current study has revealed that increases in HDAC4 and 5 in response to lipotoxicity induce transcriptional repression of oxidative metabolism and of the apoptosis and ferroptosis cell death pathways in both myogenic cells and skeletal muscle. The impairment in oxidative metabolism is directly linked to reduced metabolic inputs to the ferroptosis pathway, while increases in HDAC4 and 5 also inhibit of a pro-apoptosis transcriptional program by reducing acetylation of p53 at K120. These data indicate that metabolic reprogramming in skeletal muscle in response to lipotoxicity is directly linked with cell survival responses.

Previous findings revealed that lipotoxicity is associated with suppression of a pro-apoptosis transcriptional program in skeletal muscle, with consequences for maintenance of muscle mass(40). Our data show that the class IIa HDACs are essential for this response, as loss of HDAC4 and 5 function in skeletal muscle in a model of lipotoxicity increased apoptosis genes and markers of apoptosis, which was associated with reduced muscle mass. Furthermore, a readout of ferroptosis was also increased. The exact contribution of these cell death pathways to the reduction in muscle mass observed remains to be determined. However, inhibition of ferroptosis alone enhanced cell viability following palmitate exposure while inhibition of apoptosis alone did not, possibly revealing a greater importance of ferroptosis. The role of ferroptosis in skeletal muscle pathologies is just emerging but has been implicated in the development of sarcopenia, rhabdomyolysis and inflammatory myopathies(41). Our study also implicates skeletal muscle ferroptosis in sarcopenic obesity.

While there is much debate in the literature about the relationship between mitochondrial capacity and function and insulin action(42), the reduction in oxidative capacity induced by HDAC4 and 5 did not result in overt insulin resistance. Overexpression of HDAC4 and 5 increased basal glucose clearance, with more glucose directed to glycogen synthesis. Oxidative utilisation of glucose was impaired through the TCA cycle, particularly at the level of succinate. The levels of succinate are thought to reflect the redox state of the mitochondrial coenzyme Q pool, with higher concentrations of reduced CoQ ($CoQH_2$) preventing the oxidation of succinate by SDH(43). Oxidation of succinate by SDH is tightly associated with reverse electron flow to complex I of the electron transport chain and reduced ROS production(44). Indeed, succinate oxidation-dependent ROS production is critical for pro-inflammatory cytokine production by macrophages(45), adipose tissue thermogenesis(46) and the activity of carotid body oxygen sensing K^+ channels(47). In the context of the present study, HDAC4 and 5-mediated impairments in succinate oxidation and ROS production likely contribute to inhibition of the ferroptosis pathway and preservation of cell viability in response to lipotoxicity. Additionally, impairments in TCA cycle activity have recently been found to promote cytosolic glutathione synthesis that increases antioxidant capacity(29), which would also inhibit ferroptosis. Together, these data indicate that inhibition of oxidative substrate utilisation is an important adaptation to lipotoxicity.

In conclusion, this study provides evidence that the class IIa HDACs link impairments in skeletal muscle oxidative metabolism in response to lipotoxicity with inhibition of the apoptosis and ferroptosis cell death pathways to preserve muscle integrity. These findings provide key new insights into why certain metabolic adaptations occur in response to excess

lipids and advance our understanding of the aetiology of metabolic diseases driven by lipotoxicity and excess nutrient availability.

ACKNOWLEDGEMENTS

The authors wish to thank all members of the Metabolic Reprogramming Laboratory for helpful insights and technical advice and are grateful to the technical staff of the Deakin University Animal Services team. The authors also wish to thank Hongwei Qian for AAV production. This work was supported by grants from the National Health and Medical Research Council (NHMRC: APP1027227, APP1030474 and APP1127059) to SLM. PJM, PG and MAF are supported by Fellowships from the NHMRC.

AUTHOR CONTRIBUTIONS

Conceptualization, SDM, TC and SLM; Methodology, SDM, TC, DDS, GMK, CRB, PG, FMC, KRW and SLM; Investigation, SDM, TC, AS, KAM, DCH, BN, DDS, GMK, FMC and SLM; Resources, DLT, PJM, CRB, PG, MAF and SLM; Writing – original draft, SDM, TC and SLM; Writing – review and editing, all authors; Funding acquisition, SLM.

DECLARATION OF INTERESTS

The authors declare no competing interests related to this article.

FIGURE LEGENDS

Figure 1: HDAC4 and 5 are increased in models of lipotoxicity. (A) Heat map of ceramide (Cer), diglyceride (DG), phosphatidylcholine (PC) and triglyceride (TG) lipid species; (B) Total Cer, DG and TG lipids (One-way ANOVA; Cer $p<0.0001$ ($F(2,14)=73.86$, ^{f}Tukey's multiple comparisons test $p<0.0077$ vs. 0mM, *Tukey's multiple comparisons test $p<0.0001$ vs. 0mM and vs 0.25mM; DG $p<0.0001$ ($F(2,14)=38.50$ *Tukey's multiple comparisons test $p<0.0001$ vs. 0mM and vs 0.25mM; TG $p<0.0017$ ($F(2,14)=10.38$ *Tukey's multiple comparisons test $p=0.0333$ vs. 0mM); (C) *Ppargc1a* gene expression (One-way ANOVA $p<0.0161$ ($F(2,21)=5.054$, ^{f}Tukey's multiple comparisons test $p<0.0484$ vs. 0mM *Tukey's multiple comparisons test $p=0.0210$ vs. 0mM); (D) Oxygen consumption rate (OCR; One-way ANOVA $p<0.0255$ ($F(2,25)=4.262$ *Tukey's multiple comparisons test $p<0.0001$ vs. 0mM and vs 0.25mM), and; (E) HDAC4 and 5 protein in C2C12 myotubes treated with 0mM (BSA vehicle), 0.25mM or 0.5mM palmitate (PA) for 24 hrs (HDAC4, Kruskal-Wallis test, $p=0.049$ ($X^2 = 5.591$), *Dunn's multiple comparison test $p=0.0380$; HDAC5, One-way ANOVA, $p=0.038$ ($F(2,6)=5.903$) ^{f}Tukey's multiple comparisons test $p=0.0318$, *Tukey's multiple comparisons test $p=0.0251$). (F) Heat map of Cer, DG, PC and TG lipid species; (G) Total Cer, DG and TG lipids (Unpaired t-tests, Cer $p=0.0094$, DG $p=0.0022$, TG $p=0.0616$); (H) *Ppargc1a* gene expression (Unpaired t-test, $p=0.0357$); (I) Basal, substrate and ADP-driven OCR from muscle biopsies (Two-way ANOVA, $^{\varnothing}$genotype $p=0.0493$, $F(1,33)=4.166$), and; (J) HDAC4 and 5 protein in Control and *db/db* mice (Unpaired t-tests, $^{\#}$HDAC4 $p=0.0375$, $^{\#}$HDAC5 $p=0.0308$). Data are mean±SEM, n=3-6 biological replicates per group for cell experiments and 6-8 per group for animal experiments.

Figure 2: Overexpression of HDAC4 and 5 in skeletal muscle suppresses *Pppargc1a* expression and oxidative capacity. (A) The bilateral AAV6 HDAC4 and 5 overexpression mouse model. (B) *Hdac4* and *Hdac5* gene expression (Paired t-test, $^{\#}$*Hdac4* p=0.0246, $^{\#}$*Hdac5* p=0.0305); (C) HDAC4 and 5 protein; (D) *Ppargc1a* gene expression (Paired t-test, p=0.0006); (E) Metabolic gene expression (Paired t-test, $^{\#}$*Ppard* p=0.0055, $^{\#}$*Cpt1b* p=0.0106, $^{\#}$*Pdk4* p=0.0029, $^{\#}$*Cox7a* p=0.0087, $^{\#}$*CytC* p=0.0020, $^{\#}$*Idh1* p=0.0179, $^{\#}$*Fh* p=0.0015, $^{\#}$*Mcad* p=0.0028, $^{\#}$*Hadh* p=0.0029, $^{\#}$*Echs1* p=0.0023); (F) Respiratory chain complex subunit protein (Paired t-test, $^{\#}$Complex V p<0.0001); (G) Basal, succinate and ADP-driven oxygen consumption rate (OCR) from muscle biopsies (Two-way ANOVA, $^{\varnothing}$genotype p=0.0247, F(1,43)=5.417); (H) Basal, malate and ADP-driven OCR from muscle biopsies (Two-way ANOVA, $^{\varnothing}$genotype p=0.0036, F(1,37)=9.661), and; (I) Ceramide (Cer), diglyceride (DG), triglyceride (TG), phosphatidylethanolamine (PE), lysophosphatidylethanolamine (LPE), phosphatidylcholine (PC), lysophosphatidylcholine (LPC), phosphatidylinositol (PI), lysophosphatidylinositol (LPI), phosphoglycerol (PG) and phosphatidylserine (PS) lipids in Control and HDAC4 and 5 overexpressing skeletal muscle. Data are mean±SEM, n=4-6 per group.

Figure 3: Overexpression of HDAC4 and 5 in skeletal muscle inhibits oxidative glucose utilisation. (A) Experimental overview of insulin and isotopic glucose tracers in the bilateral AAV6 HDAC4 and 5 overexpression model. (B) Glucose clearance (Two-way ANOVA, $^{\varnothing}$genotype p=0.0328, F(1,27)=5.061); (C) Glucose clearance in muscle overexpressing HDAC4 and 5 relative to Control (Paired t-test, $^{\#}$Vehicle p=0.0355); (D) ^{14}C-glucose incorporation into glycogen (Two-way ANOVA, $^{\varnothing}$genotype p=0.0372, F(1,24)=4.864); (E) ^{14}C-glucose incorporation into lipid (Two-way ANOVA, ^Insulin p=0.0009, F(1,21)=14.94); (F) Representative images of insulin signalling components; (G) pT308 Akt (Two-way ANOVA, ^Insulin p=0.0010, F(1,27)=13.75); (H) pS473 Akt (Two-way ANOVA, ^Insulin p<0.0001, F(1,28)=33.13), and; (I) pS642 TBC1D4 (Two-way ANOVA, $^{\varnothing}$genotype p=0.0011, F(1,25)=13.60) in bilateral AAV6 HDAC4 and 5 mice administered insulin and isotopic glucose tracers. (J) Experimental overview of stable isotope metabolomics in the bilateral AAV6 HDAC4 and 5 overexpression model. (K) Total metabolite abundance (Paired t-test, $^{\#}$Lactate p=0.0447, $^{\#}$Succinate p=0.0355); (L) Total ^{13}C labelling of glycolytic and TCA cycle metabolites (Paired t-test, $^{\#}$Succinate p=0.0447, $^{\#}$Malate p=0.0355); (M) Lactate isotopologue (Paired t-test, $^{\#}$M0 p=0.0448, $^{\#}$M2 p=0.0299); (N) Succinate isotopologues (Paired t-test, $^{\#}$M0 p=0.0230, $^{\#}$M1 p=0.0002, $^{\#}$M2 p=0.0005), and; (O) Malate isotopologues (Paired t-test, $^{\#}$M1 p=0.0178) in bilateral AAV6 HDAC4 and 5 mice administered ^{13}C- glucose tracer. (E) Data are mean±SEM, n=5-8 per group.

Figure 4: HDAC and 5 enhance cell survival in response to lipotoxicity and supress the apoptosis and ferroptosis cell death pathways. (A) Expression of p53-pathway genes involved in pro-apoptosis, anti-apoptosis, intrinsic apoptosis and ferroptosis (Unpaired t-test, $^{\#}$*Casp3* p=0.0451, $^{\#}$*Casp9* p=0.0057, $^{\#}$*Cycs* p=0.0015, $^{\#}$*Pmaip1* p<0.0001, $^{\#}$*Bbc3* p=0.0253, $^{\#}$*Bcl2* p=0.0034, $^{\#}$*Bcl2l1* p=0.0008, $^{\#}$*Slc7a11* p<0.0001, $^{\#}$*Sat1* p<0.0001, $^{\#}$*Alox15* p=0.0001); (B) Apoptotic cells in response to the apoptosis-inducing agent Camptothecin (Two-way ANOVA, genotype p<0.0001 F(1,12)=349.3, treatment p<0.0001 F(2,12)=270.4, interaction p<0.0001 F(2,12)=149.5; $^{\#}$p<0.05 vs Control for same treatment, *p<0.05 vs vehicle by Tukey's multiple comparisons tests); (C) Cell viability in response to the ferroptosis-inducing agent RSL3 (Two-way ANOVA, genotype p<0.0001 F(1,12)=1645, treatment p<0.0001 F(1,12)=36.09, interaction p<0.0090 F(1,12)=9.665; $^{\#}$p<0.05 vs Control for same treatment, *p<0.05 vs 0.25μM RSL by Tukey's multiple comparisons tests); (D) Cell viability in response to palmitate (Two-way ANOVA, genotype p<0.0001 F(1,12)=3374, treatment p<0.0001 F(2,12)=1012, interaction p<0.0001 F(2,12)=684.8; $^{\#}$p<0.05 vs Control for same treatment, *p<0.05 vs vehicle by Tukey's multiple comparisons tests); (E) Full-length (FL) and cleaved (CL) caspase 3 and 9 in response to palmitate; (F) Apoptotic cells in response to palmitate (Two-way ANOVA, genotype p<0.0001 F(1,12)=1468, treatment p=0.0001 F(2,12)=20.35, interaction p<0.0050 F(2,12)=8.498; $^{\#}$p<0.05 vs Control for same treatment, *p<0.05 vs vehicle by Tukey's multiple comparisons tests); (G) Lipid peroxidation in response to palmitate (Two-way ANOVA, genotype p<0.0001 F(1,12)=313.4, treatment p<0.0103 F(2,12)=67.31; $^{\#}$p<0.05 vs Control for same treatment by Tukey's multiple comparisons tests) in Control and HDAC4 and 5 overexpressing C2C12 myoblasts. Data are mean±SEM, n=3-4 biological replicates per group.

Figure 5: HDAC4 and 5 inhibit apoptosis by reducing p53 K120 acetylation and reduces multiple metabolic inputs to the ferroptosis pathway. (A) Acetylated p53 at lysine 120 (aK120 p53); (B) Expression of caspase 3 (*Casp3;* One-way ANOVA p=0.0040 X^2=0.8408, ^p<0.05 vs Control + WT p53 and HDAC4&5 + K120Q p53 by Tukey's multiple comparisons test), caspase 9 (*Casp9;* One-way ANOVA p=0.0025 X^2=0.8650, ^p<0.05 vs Control + WT p53 and HDAC4&5 + K120Q p53 by Tukey's multiple comparisons test), cytochrome c (*Cycs;* One-way ANOVA p=0.0033 X^2=0.8518, ^p<0.05 vs Control + WT p53 by Tukey's multiple comparisons test) and the cystine/glutamate antiporter xCT (*Slc7a11;* One-way ANOVA p<0.0001 X^2=0.9769, ^p<0.05 vs Control + WT p53 by Tukey's multiple comparisons test); (C) Percentage of apoptotic cells following exposure to camptothecin (One-way ANOVA p=0.0014 X^2=0.8875, ^p<0.05 vs Control + WT p53 and HDAC4&5 + K120Q p53 by Tukey's multiple comparisons test); (D) Cell viability 16 hrs after palmitate exposure (Two-way ANOVA, treatment p<0.0001 F(1,12)=50.44, genotype p=0.0361 F(1,12)=5.56; *p<0.05 vs vehicle for same genotype by Tukey's multiple comparisons tests) in C2C12 myoblasts expressing wild type (WT) or K120R (loss-of-function) p53 treated with vehicle or 2mM palmitate for 24 hrs. (E) Cell viability following palmitate exposure and co-incubation with vehicle (DMSO) or increasing concentrations of Z-DEVD-FMK (One-way ANOVA p=0.3282); (F) Schematic showing key regulatory points in the ferroptosis pathway; (G) Cell viability following palmitate exposure and co-incubation with vehicle (DMSO) or increasing concentrations of Ferrostatin (One-way ANOVA p=0.0323 X^2=0.5337, *p<0.05 vs Vehicle by Tukey's multiple comparisons test); (H) Cell viability following exposure to increasing concentrations of Erastin (Two-way ANOVA, genotype p<0.0001 F(1,18)=293.7, treatment p<0.0001 F(2,18)=139.6, interaction p<0.0001 F(2,18)=50.88; $^{\#}$p<0.05 vs Control for same treatment, *p<0.05 vs Vehicle same genotype by Tukey's multiple comparisons tests); (I) Glutamate (Glu), glutathione (GSH) and

the GSH/Glu ratio (Unpaired t-tests, #Glu p=0.0049, #GSH/Glu p=0.0023); (J) Glutathione peroxidase (GPX) activity (Unpaired t-test, p<0.0001), and; (K) H_2O_2 derived from mitochondria (mito), NADPH oxidases (NOX) and other sources (Unpaired t-tests, #Mito p=0.0105, #NAPDH Ox. p<0.0001, #Other p=0.0004) in Control or HDAC4 and 5 overexpressing C2C12 myoblasts. Data are mean±SEM, n=4-10 biological replicates per group.

Figure 6: HDAC4 and 5 are required to suppress apoptosis and ferroptosis and maintain muscle mass in obese mice. (A) The bilateral AAV6 dominant negative (DN) HDAC4 and 5 overexpression *db/db* mouse model. (B) *Hdac4* and *Hdac5* gene expression (Paired t-tests, #*Hdac4* p=0.0003, #*Hdac5* p=0.0002); (C) HDAC4 and 5 protein; (D) *Ppargc1a* gene expression (Paired t-tests, p=0.0191); (E) Basal, substrate and ADP-driven oxygen consumption rate (OCR) from muscle biopsies (Two-way ANOVA, genotype p=0.0482 $F(1,42)=4.141$); (F) Caspase 3 activity (Paired t-tests, p=0.0292); (G) Lipid peroxidation (Paired t-tests, p=0.0013); (H) Acetylated p53 at lysine 120 (aK120 p53); (I) Expression of apoptosis genes (Paired t-tests, #*Casp3* p=0.0036, #*Casp9* p=0.0064, #*Bbc3* p=0.0024); (J) Reactive oxygen species (ROS; Paired t-tests, p=0.0292); (K) Expression of ferroptosis genes (Paired t-tests, #*Sat1* p=0.0257, #*Casp9* p=0.0286); (L) Mass of the gastrocnemius (Gastroc.) and tibialis anterior (TA) skeletal muscles (Paired t-tests, #Gastroc. P<0.0001, #TA p=0.0004); (M) Masson's trichrome staining, and; (N) H&E staining of sections of the TA muscle in Control and DN HDAC4 and 5 overexpressing skeletal muscle in *db/db* mice. Arrows indicate fibres with centralised nuclei. Data are mean±SEM, n=6-10 per group.

REFERENCES

1. Lee Y, Hirose H, Ohneda M, Johnson JH, McGarry JD, Unger RH: Beta-cell lipotoxicity in the pathogenesis of non-insulin-dependent diabetes mellitus of obese rats: impairment in adipocyte-beta-cell relationships. Proceedings of the National Academy of Sciences of the United States of America 1994;91:10878-10882

2. Schaffer JE: Lipotoxicity: when tissues overeat. Current opinion in lipidology 2003;14:281-287

3. Kelley DE, Simoneau JA: Impaired free fatty acid utilization by skeletal muscle in non-insulin-dependent diabetes mellitus. The Journal of clinical investigation 1994;94:2349-2356

4. Simoneau JA, Kelley DE: Altered glycolytic and oxidative capacities of skeletal muscle contribute to insulin resistance in NIDDM. Journal of applied physiology 1997;83:166-171

5. Baker PR, 2nd, Boyle KE, Koves TR, Ilkayeva OR, Muoio DM, Houmard JA, Friedman JE: Metabolomic analysis reveals altered skeletal muscle amino acid and fatty acid handling in obese humans. Obesity (Silver Spring) 2015;23:981-988

6. Lerin C, Goldfine AB, Boes T, Liu M, Kasif S, Dreyfuss JM, De Sousa-Coelho AL, Daher G, Manoli I, Sysol JR, Isganaitis E, Jessen N, Goodyear LJ, Beebe K, Gall W, Venditti CP, Patti ME: Defects in muscle branched-chain amino acid oxidation contribute to impaired lipid metabolism. Molecular metabolism 2016;5:926-936

7. White PJ, Lapworth AL, An J, Wang L, McGarrah RW, Stevens RD, Ilkayeva O, George T, Muehlbauer MJ, Bain JR, Trimmer JK, Brosnan MJ, Rolph TP, Newgard CB: Branched-chain amino acid restriction in Zucker-fatty rats improves muscle insulin sensitivity by enhancing efficiency of fatty acid oxidation and acyl-glycine export. Molecular metabolism 2016;5:538-551

8. Dube JJ, Coen PM, DiStefano G, Chacon AC, Helbling NL, Desimone ME, Stafanovic-Racic M, Hames KC, Despines AA, Toledo FG, Goodpaster BH: Effects of acute lipid overload on skeletal muscle insulin resistance, metabolic flexibility, and mitochondrial performance. American journal of physiology Endocrinology and metabolism 2014;307:E1117-1124

9. Richardson DK, Kashyap S, Bajaj M, Cusi K, Mandarino SJ, Finlayson J, DeFronzo RA, Jenkinson CP, Mandarino LJ: Lipid infusion decreases the expression of nuclear encoded mitochondrial genes and increases the expression of extracellular matrix genes in human skeletal muscle. The Journal of biological chemistry 2005;280:10290-10297

10. Sparks LM, Xie H, Koza RA, Mynatt R, Hulver MW, Bray GA, Smith SR: A high-fat diet coordinately downregulates genes required for mitochondrial oxidative phosphorylation in skeletal muscle. Diabetes 2005;54:1926-1933

11. Gaur V, Connor T, Sanigorski A, Martin SD, Bruce CR, Henstridge DC, Bond ST, McEwen KA, Kerr-Bayles L, Ashton TD, Fleming C, Wu M, Pike Winer LS, Chen D, Hudson GM, Schwabe JW, Baar K, Febbraio MA, Gregorevic P, Pfeffer FM, Walder KR, Hargreaves M, McGee SL: Disruption of the Class IIa HDAC Corepressor Complex Increases Energy Expenditure and Lipid Oxidation. Cell reports 2016;16:2802-2810

12. Czubryt MP, McAnally J, Fishman GI, Olson EN: Regulation of peroxisome proliferator-activated receptor gamma coactivator 1 alpha (PGC-1 alpha) and mitochondrial function by MEF2 and HDAC5. Proceedings of the National Academy of Sciences of the United States of America 2003;100:1711-1716

13. Backs J, Backs T, Bezprozvannaya S, McKinsey TA, Olson EN: Histone deacetylase 5 acquires calcium/calmodulin-dependent kinase II responsiveness by oligomerization with histone deacetylase 4. Molecular and cellular biology 2008;28:3437-3445

14. Lemercier C, Verdel A, Galloo B, Curtet S, Brocard MP, Khochbin S: mHDA1/HDAC5 histone deacetylase interacts with and represses MEF2A transcriptional activity. The Journal of biological chemistry 2000;275:15594-15599

15. McKinsey TA, Zhang CL, Lu J, Olson EN: Signal-dependent nuclear export of a histone deacetylase regulates muscle differentiation. Nature 2000;408:106-111

16. McGee SL, van Denderen BJ, Howlett KF, Mollica J, Schertzer JD, Kemp BE, Hargreaves M: AMP-activated protein kinase regulates GLUT4 transcription by phosphorylating histone deacetylase 5. Diabetes 2008;57:860-867

17. Mihaylova MM, Vasquez DS, Ravnskjaer K, Denechaud PD, Yu RT, Alvarez JG, Downes M, Evans RM, Montminy M, Shaw RJ: Class IIa histone deacetylases are hormone-activated regulators of FOXO and mammalian glucose homeostasis. Cell 2011;145:607-621

18. McGee SL, Swinton C, Morrison S, Gaur V, Campbell DE, Jorgensen SB, Kemp BE, Baar K, Steinberg GR, Hargreaves M: Compensatory regulation of HDAC5 in muscle maintains metabolic adaptive responses and metabolism in response to energetic stress. FASEB journal : official publication of the Federation of American Societies for Experimental Biology 2014;28:3384-3395

19. McGee SL, Fairlie E, Garnham AP, Hargreaves M: Exercise-induced histone modifications in human skeletal muscle. The Journal of physiology 2009;587:5951-5958

20. Martin SD, Morrison S, Konstantopoulos N, McGee SL: Mitochondrial dysfunction has divergent, cell type-dependent effects on insulin action. Molecular metabolism 2014;3:408-418

21. Genders AJ, Connor T, Morrison S, Bond ST, Drew BG, Meikle PJ, Howlett KF, McGee SL: Reducing hepatic PKD activity lowers circulating VLDL cholesterol. J Endocrinol 2020;246:265-276

22. Hortle E, Nijagal B, Bauer DC, Jensen LM, Ahn SB, Cockburn IA, Lampkin S, Tull D, McConville MJ, McMorran BJ, Foote SJ, Burgio G: Adenosine monophosphate deaminase 3 activation shortens erythrocyte half-life and provides malaria resistance in mice. Blood 2016;128:1290-1301

23. McGee SL, Hargreaves M: Exercise and myocyte enhancer factor 2 regulation in human skeletal muscle. Diabetes 2004;53:1208-1214

24. De Jong KA, Hall LG, Renton MC, Connor T, Martin SD, Kowalski GM, Shaw CS, Bruce CR, Howlett KF, McGee SL: Loss of protein kinase D activity demonstrates redundancy in cardiac glucose metabolism and preserves cardiac function in obesity. Molecular metabolism 2020;42:101105

25. Patti ME, Butte AJ, Crunkhorn S, Cusi K, Berria R, Kashyap S, Miyazaki Y, Kohane I, Costello M, Saccone R, Landaker EJ, Goldfine AB, Mun E, DeFronzo R, Finlayson J, Kahn CR, Mandarino LJ: Coordinated reduction of genes of oxidative metabolism in humans with insulin resistance and diabetes: Potential role of PGC1 and NRF1. Proceedings of the National Academy of Sciences of the United States of America 2003;100:8466-8471

26. Petersen KF, Dufour S, Befroy D, Garcia R, Shulman GI: Impaired mitochondrial activity in the insulin-resistant offspring of patients with type 2 diabetes. The New England journal of medicine 2004;350:664-671

27. Kowalski GM, De Souza DP, Burch ML, Hamley S, Kloehn J, Selathurai A, Tull D, O'Callaghan S, McConville MJ, Bruce CR: Application of dynamic metabolomics to examine in vivo skeletal muscle glucose metabolism in the chronically high-fat fed mouse. Biochemical and biophysical research communications 2015;462:27-32

28. Zhang W, Guo C, Jiang K, Ying M, Hu X: Quantification of lactate from various metabolic pathways and quantification issues of lactate isotopologues and isotopmers. Sci Rep 2017;7:8489

29. Ryan DG, Yang M, Prag HA, Blanco GR, Nikitopoulou E, Segarra-Mondejar M, Powell CA, Young T, Burger N, Miljkovic JL, Minczuk M, Murphy MP, von Kriegsheim A, Frezza C: Disruption of the TCA cycle reveals an ATF4-dependent integration of redox and amino acid metabolism. Elife 2021;10

30. Jiang X, Stockwell BR, Conrad M: Ferroptosis: mechanisms, biology and role in disease. Nature reviews Molecular cell biology 2021;22:266-282

31. Sykes SM, Mellert HS, Holbert MA, Li K, Marmorstein R, Lane WS, McMahon SB: Acetylation of the p53 DNA-binding domain regulates apoptosis induction. Molecular cell 2006;24:841-851

32. Tang Y, Luo J, Zhang W, Gu W: Tip60-dependent acetylation of p53 modulates the decision between cell-cycle arrest and apoptosis. Molecular cell 2006;24:827-839

33. Sen N, Kumari R, Singh MI, Das S: HDAC5, a key component in temporal regulation of p53-mediated transactivation in response to genotoxic stress. Molecular cell 2013;52:406-420

34. Jiang L, Kon N, Li T, Wang SJ, Su T, Hibshoosh H, Baer R, Gu W: Ferroptosis as a p53-mediated activity during tumour suppression. Nature 2015;520:57-62

35. Berkers CR, Maddocks OD, Cheung EC, Mor I, Vousden KH: Metabolic regulation by p53 family members. Cell metabolism 2013;18:617-633

36. Stockwell BR, Friedmann Angeli JP, Bayir H, Bush AI, Conrad M, Dixon SJ, Fulda S, Gascon S, Hatzios SK, Kagan VE, Noel K, Jiang X, Linkermann A, Murphy ME, Overholtzer M, Oyagi A, Pagnussat GC, Park J, Ran Q, Rosenfeld CS, Salnikow K, Tang D, Torti FM, Torti SV, Toyokuni S,

Woerpel KA, Zhang DD: Ferroptosis: A Regulated Cell Death Nexus Linking Metabolism, Redox Biology, and Disease. Cell 2017;171:273-285

37. Kagan VE, Mao G, Qu F, Angeli JP, Doll S, Croix CS, Dar HH, Liu B, Tyurin VA, Ritov VB, Kapralov AA, Amoscato AA, Jiang J, Anthonymuthu T, Mohammadyani D, Yang Q, Proneth B, Klein-Seetharaman J, Watkins S, Bahar I, Greenberger J, Mallampalli RK, Stockwell BR, Tyurina YY, Conrad M, Bayir H: Oxidized arachidonic and adrenic PEs navigate cells to ferroptosis. Nature chemical biology 2017;13:81-90

38. Ou Y, Wang SJ, Li D, Chu B, Gu W: Activation of SAT1 engages polyamine metabolism with p53-mediated ferroptotic responses. Proceedings of the National Academy of Sciences of the United States of America 2016;113:E6806-E6812

39. Piccolis M, Bond LM, Kampmann M, Pulimeno P, Chitraju C, Jayson CBK, Vaites LP, Boland S, Lai ZW, Gabriel KR, Elliott SD, Paulo JA, Harper JW, Weissman JS, Walther TC, Farese RV, Jr.: Probing the Global Cellular Responses to Lipotoxicity Caused by Saturated Fatty Acids. Molecular cell 2019;74:32-44 e38

40. Turpin SM, Ryall JG, Southgate R, Darby I, Hevener AL, Febbraio MA, Kemp BE, Lynch GS, Watt MJ: Examination of 'lipotoxicity' in skeletal muscle of high-fat fed and ob/ob mice. The Journal of physiology 2009;587:1593-1605

41. Wang Y, Zhang Z, Jiao W, Wang Y, Wang X, Zhao Y, Fan X, Tian L, Li X, Mi J: Ferroptosis and its role in skeletal muscle diseases. Front Mol Biosci 2022;9:1051866

42. Muoio DM, Neufer PD: Lipid-induced mitochondrial stress and insulin action in muscle. Cell metabolism 2012;15:595-605

43. Murphy MP, Chouchani ET: Why succinate? Physiological regulation by a mitochondrial coenzyme Q sentinel. Nature chemical biology 2022;18:461-469

44. Chance B, Hollunger G: The interaction of energy and electron transfer reactions in mitochondria. I. General properties and nature of the products of succinate-linked reduction of pyridine nucleotide. The Journal of biological chemistry 1961;236:1534-1543

45. Mills EL, Kelly B, Logan A, Costa ASH, Varma M, Bryant CE, Tourlomousis P, Dabritz JHM, Gottlieb E, Latorre I, Corr SC, McManus G, Ryan D, Jacobs HT, Szibor M, Xavier RJ, Braun T, Frezza C, Murphy MP, O'Neill LA: Succinate Dehydrogenase Supports Metabolic Repurposing of Mitochondria to Drive Inflammatory Macrophages. Cell 2016;167:457-470 e413

46. Mills EL, Pierce KA, Jedrychowski MP, Garrity R, Winther S, Vidoni S, Yoneshiro T, Spinelli JB, Lu GZ, Kazak L, Banks AS, Haigis MC, Kajimura S, Murphy MP, Gygi SP, Clish CB, Chouchani ET: Accumulation of succinate controls activation of adipose tissue thermogenesis. Nature 2018;560:102-106

47. Fernandez-Aguera MC, Gao L, Gonzalez-Rodriguez P, Pintado CO, Arias-Mayenco I, Garcia-Flores P, Garcia-Perganeda A, Pascual A, Ortega-Saenz P, Lopez-Barneo J: Oxygen Sensing by Arterial Chemoreceptors Depends on Mitochondrial Complex I Signaling. Cell metabolism 2015;22:825-837

FIGURE 1

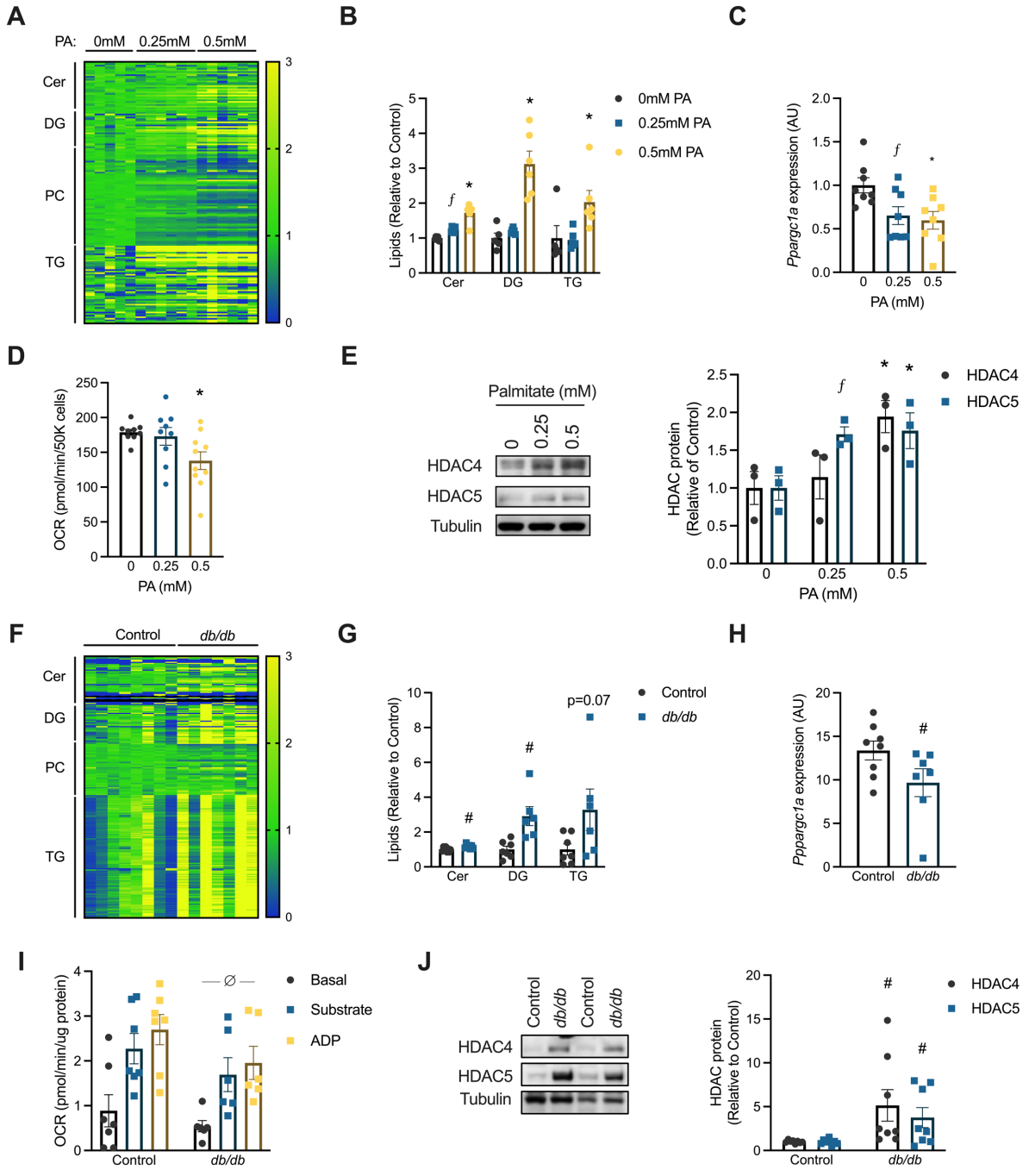
A
PA: 0mM 0.25mM 0.5mM
Cer
DG
PC
TG
B
Lipids (Relative to Control)
Cer DG TG
0mM PA
0.25mM PA
0.5mM PA
C
Ppargc1a expression (AU)
PA (mM)
D
OCR (pmol/min/50K cells)
PA (mM)
E
Palmitate (mM)
0 0.25 0.5
HDAC4
HDAC5
Tubulin
HDAC protein (Relative of Control)
PA (mM)
F
Control db/db
Cer
DG
PC
TG
G
Lipids (Relative to Control)
p=0.07
Control
db/db
H
Ppargc1a expression (AU)
Control db/db
I
OCR (pmol/min/ug protein)
Basal
Substrate
ADP
Control db/db
J
Control db/db Control db/db
HDAC4
HDAC5
Tubulin
HDAC protein (Relative to Control)
Control db/db

FIGURE 2

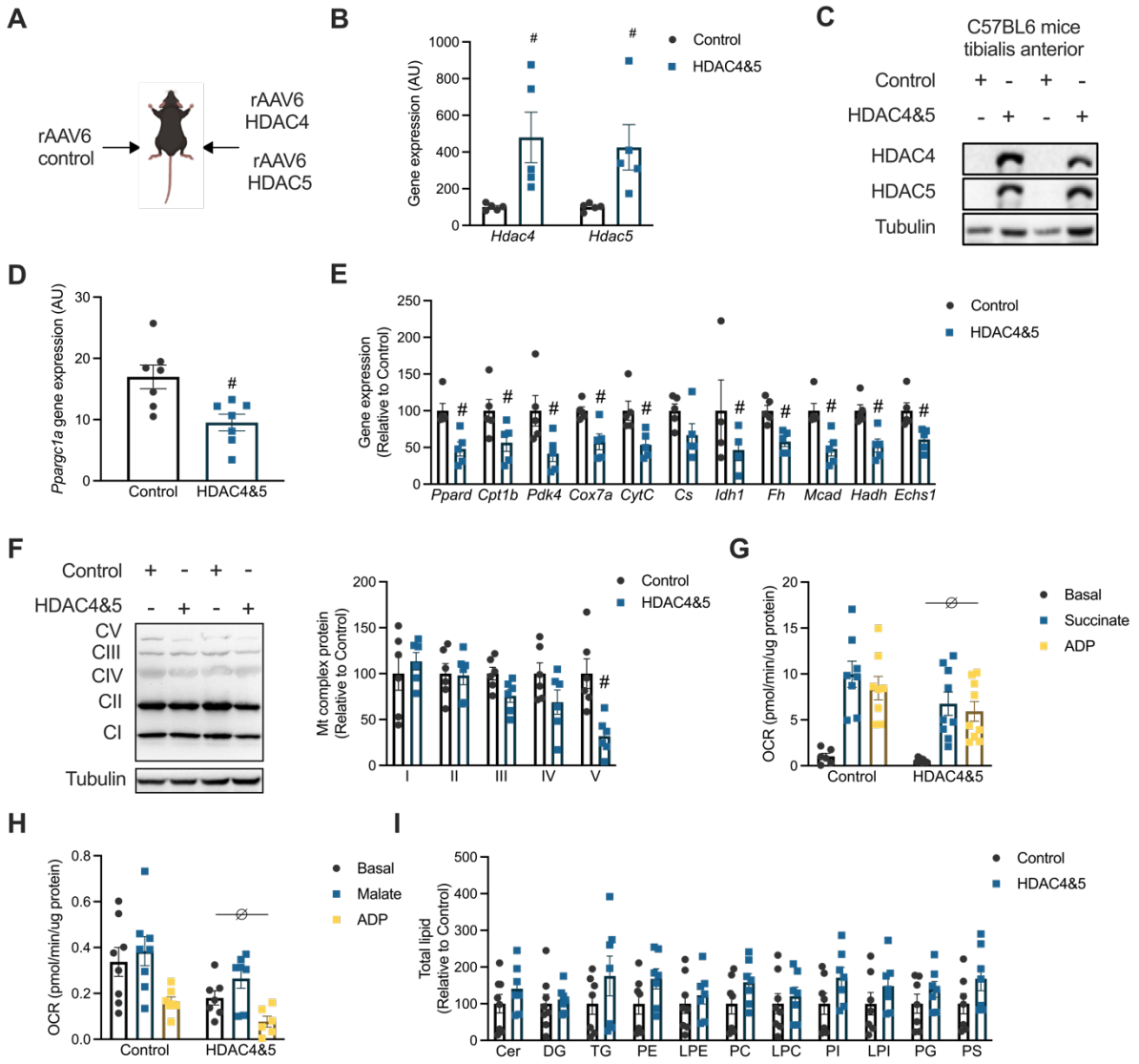
A
rAAV6 control
rAAV6 HDAC4
rAAV6 HDAC5
B
Gene expression (AU)
Hdac4
Hdac5
Control
HDAC4&5
C
C57BL6 mice tibialis anterior
Control
HDAC4&5
HDAC4
HDAC5
Tubulin
D
Ppargc1a gene expression (AU)
Control
HDAC4&5
E
Gene expression (Relative to Control)
Ppard
Cpt1b
Pdk4
Cox7a
CytC
Cs
Idh1
Fh
Mcad
Hadh
Echs1
Control
HDAC4&5
F
Control
HDAC4&5
CV
CIII
CIV
CII
CI
Tubulin
Mt complex protein (Relative to Control)
I
II
III
IV
V
Control
HDAC4&5
G
OCR (pmol/min/ug protein)
Control
HDAC4&5
Basal
Succinate
ADP
H
OCR (pmol/min/ug protein)
Control
HDAC4&5
Basal
Malate
ADP
I
Total lipid (Relative to Control)
Cer
DG
TG
PE
LPE
PC
LPC
PI
LPI
PG
PS
Control
HDAC4&5

FIGURE 3

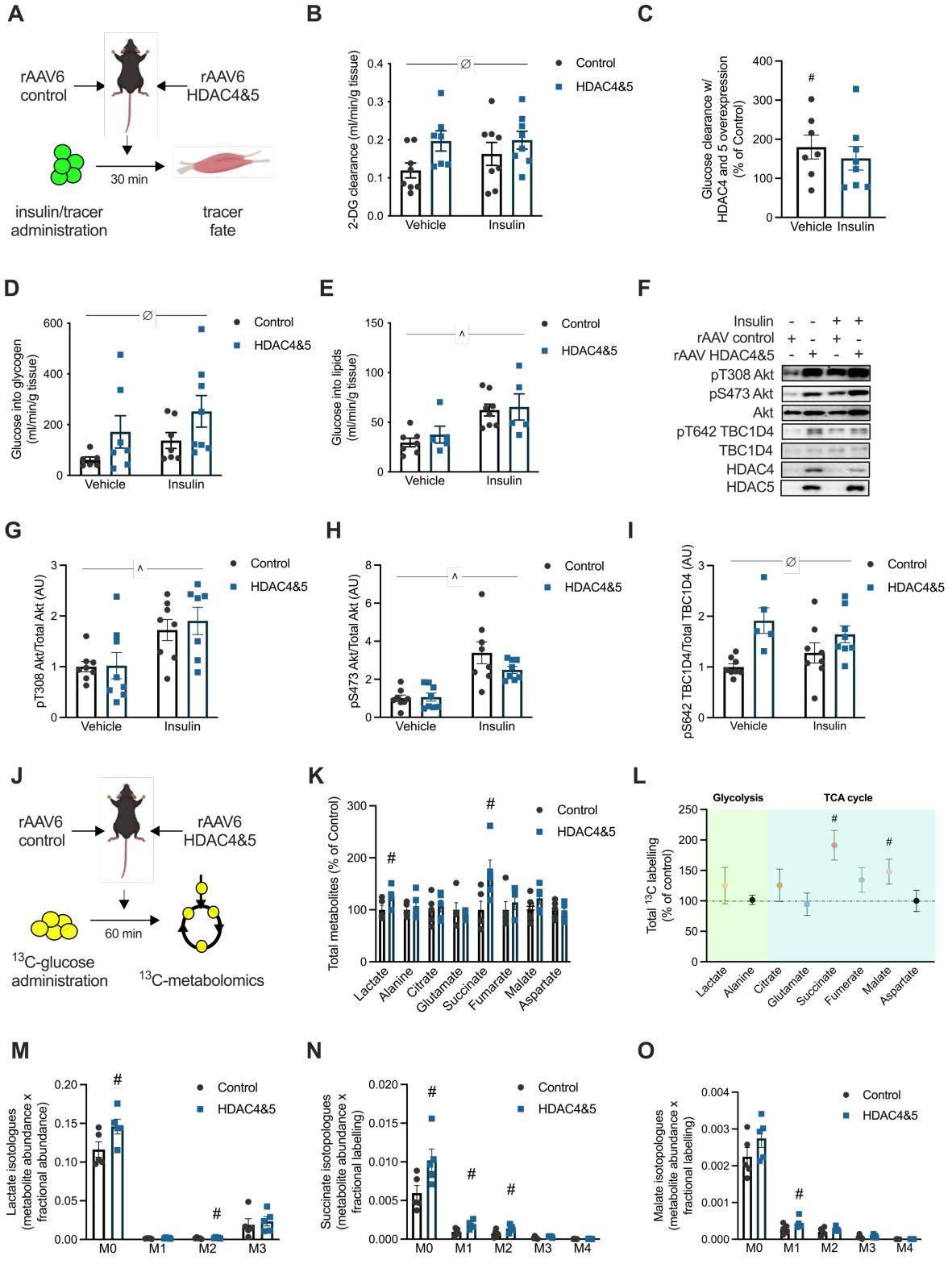
A
rAAV6 control
rAAV6 HDAC4&5
30 min
insulin/tracer administration
tracer fate
B
2-DG clearance (ml/min/g tissue)
Control
HDAC4&5
Vehicle
Insulin
C
Glucose clearance w/ HDAC4 and 5 overexpression (% of Control)
Vehicle
Insulin
D
Glucose into glycogen (ml/min/g tissue)
Control
HDAC4&5
Vehicle
Insulin
E
Glucose into lipids (ml/min/g tissue)
Control
HDAC4&5
Vehicle
Insulin
F
Insulin
rAAV control
rAAV HDAC4&5
pT308 Akt
pS473 Akt
Akt
pT642 TBC1D4
TBC1D4
HDAC4
HDAC5
G
pT308 Akt/Total Akt (AU)
Control
HDAC4&5
Vehicle
Insulin
H
pS473 Akt/Total Akt (AU)
Control
HDAC4&5
Vehicle
Insulin
I
pS642 TBC1D4/Total TBC1D4 (AU)
Control
HDAC4&5
Vehicle
Insulin
J
rAAV6 control
rAAV6 HDAC4&5
60 min
13C-glucose administration
13C-metabolomics
K
Total metabolites (% of Control)
Control
HDAC4&5
Lactate
Alanine
Citrate
Glutamate
Succinate
Fumarate
Malate
Aspartate
L
Glycolysis
TCA cycle
Total 13C labelling (% of control)
Lactate
Alanine
Citrate
Glutamate
Succinate
Fumerate
Malate
Aspartate
M
Lactate isotologues (metabolite abundance x fractional abundance)
Control
HDAC4&5
M0
M1
M2
M3
N
Succinate isotopologues (metabolite abundance x fractional labelling)
Control
HDAC4&5
M0
M1
M2
M3
M4
O
Malate isotopologues (metabolite abundance x fractional labelling)
Control
HDAC4&5
M0
M1
M2
M3
M4

FIGURE 4

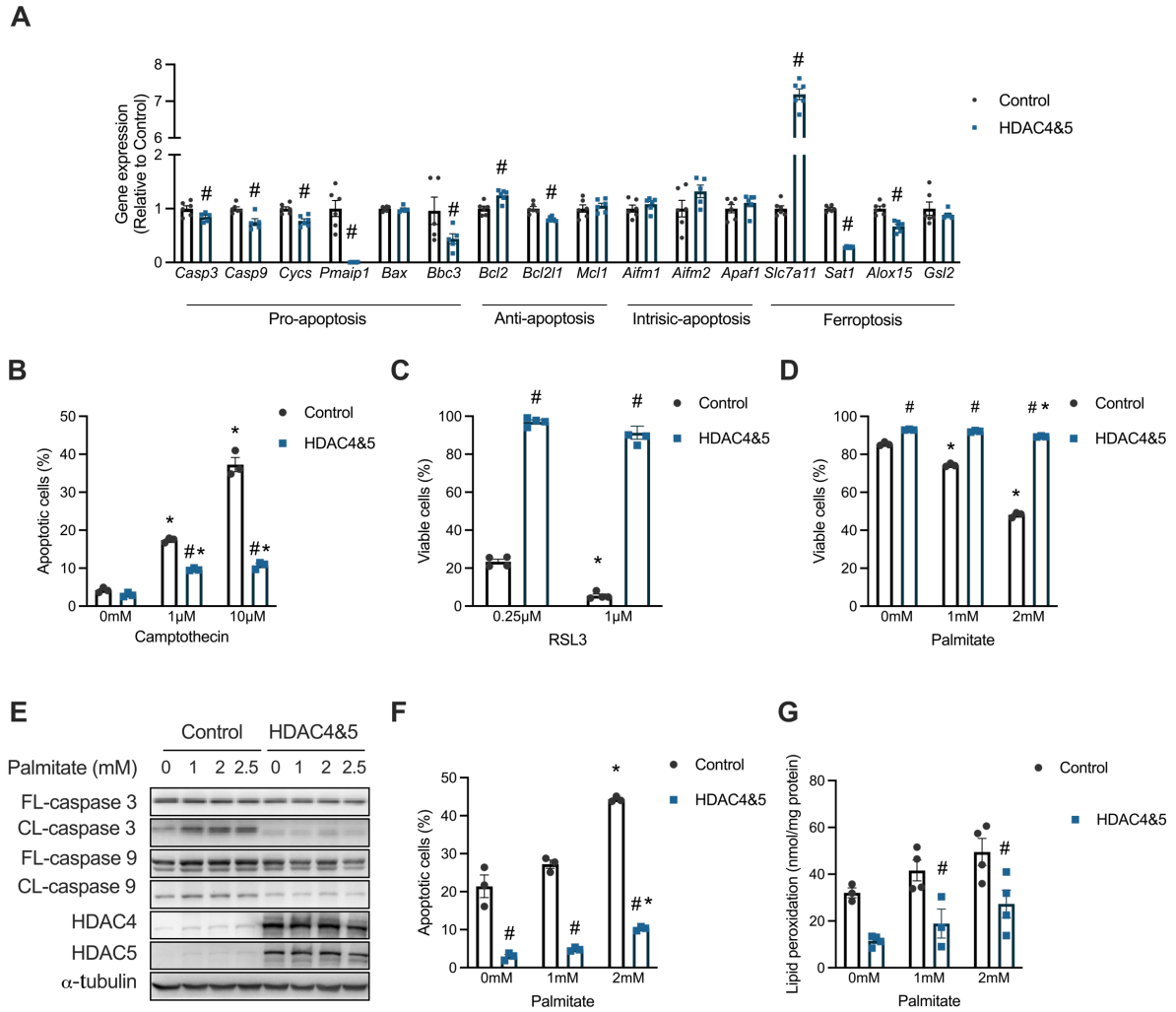
A
Gene expression (Relative to Control)
Control
HDAC4&5
Casp3 Casp9 Cycs Pmaip1 Bax Bbc3 Bcl2 Bcl2l1 Mcl1 Aifm1 Aifm2 Apaf1 Slc7a11 Sat1 Alox15 Gsl2
Pro-apoptosis
Anti-apoptosis
Intrisic-apoptosis
Ferroptosis
B
Apoptotic cells (%)
0mM 1μM 10μM
Camptothecin
C
Viable cells (%)
0.25μM 1μM
RSL3
D
Viable cells (%)
0mM 1mM 2mM
Palmitate
E
Control HDAC4&5
Palmitate (mM) 0 1 2 2.5 0 1 2 2.5
FL-caspase 3
CL-caspase 3
FL-caspase 9
CL-caspase 9
HDAC4
HDAC5
α-tubulin
F
Apoptotic cells (%)
0mM 1mM 2mM
Palmitate
G
Lipid peroxidation (nmol/mg protein)
0mM 1mM 2mM
Palmitate

FIGURE 5

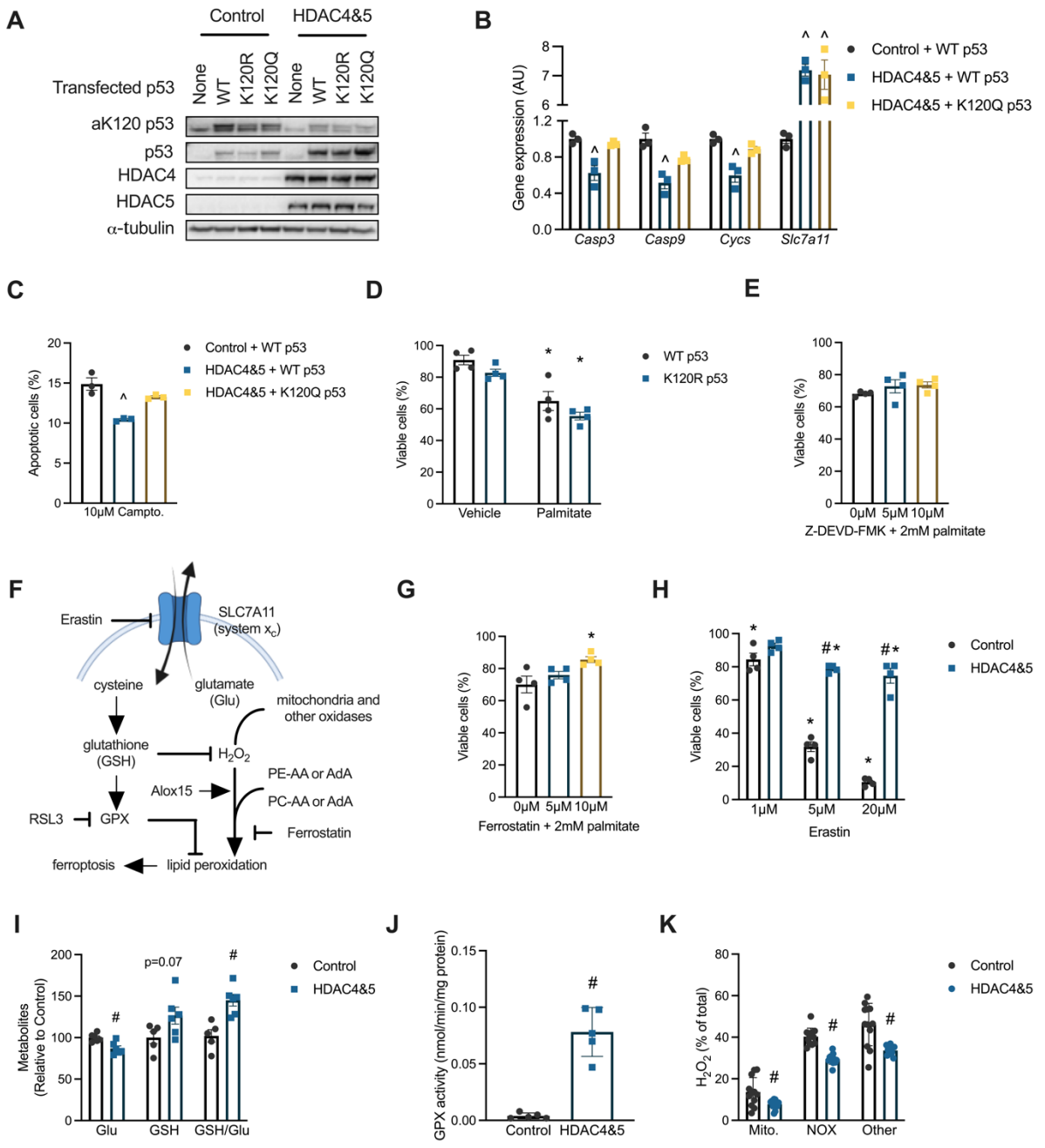
A
Control
HDAC4&5
Transfected p53
None
WT
K120R
K120Q
None
WT
K120R
K120Q
aK120 p53
p53
HDAC4
HDAC5
α-tubulin
B
Gene expression (AU)
Control + WT p53
HDAC4&5 + WT p53
HDAC4&5 + K120Q p53
Casp3
Casp9
Cycs
Slc7a11
C
Apoptotic cells (%)
10μM Campto.
D
Viable cells (%)
WT p53
K120R p53
Vehicle
Palmitate
E
Viable cells (%)
0μM 5μM 10μM
Z-DEVD-FMK + 2mM palmitate
F
Erastin
SLC7A11
(system xc)
cysteine
glutamate
(Glu)
mitochondria and
other oxidases
glutathione
(GSH)
H2O2
PE-AA or AdA
Alox15
PC-AA or AdA
RSL3
GPX
Ferrostatin
ferroptosis
lipid peroxidation
G
Viable cells (%)
0μM 5μM 10μM
Ferrostatin + 2mM palmitate
H
Viable cells (%)
Control
HDAC4&5
1μM
5μM
20μM
Erastin
I
Metabolites
(Relative to Control)
p=0.07
Control
HDAC4&5
Glu
GSH
GSH/Glu
J
GPX activity (nmol/min/mg protein)
Control
HDAC4&5
K
H2O2 (% of total)
Control
HDAC4&5
Mito.
NOX
Other

FIGURE 6

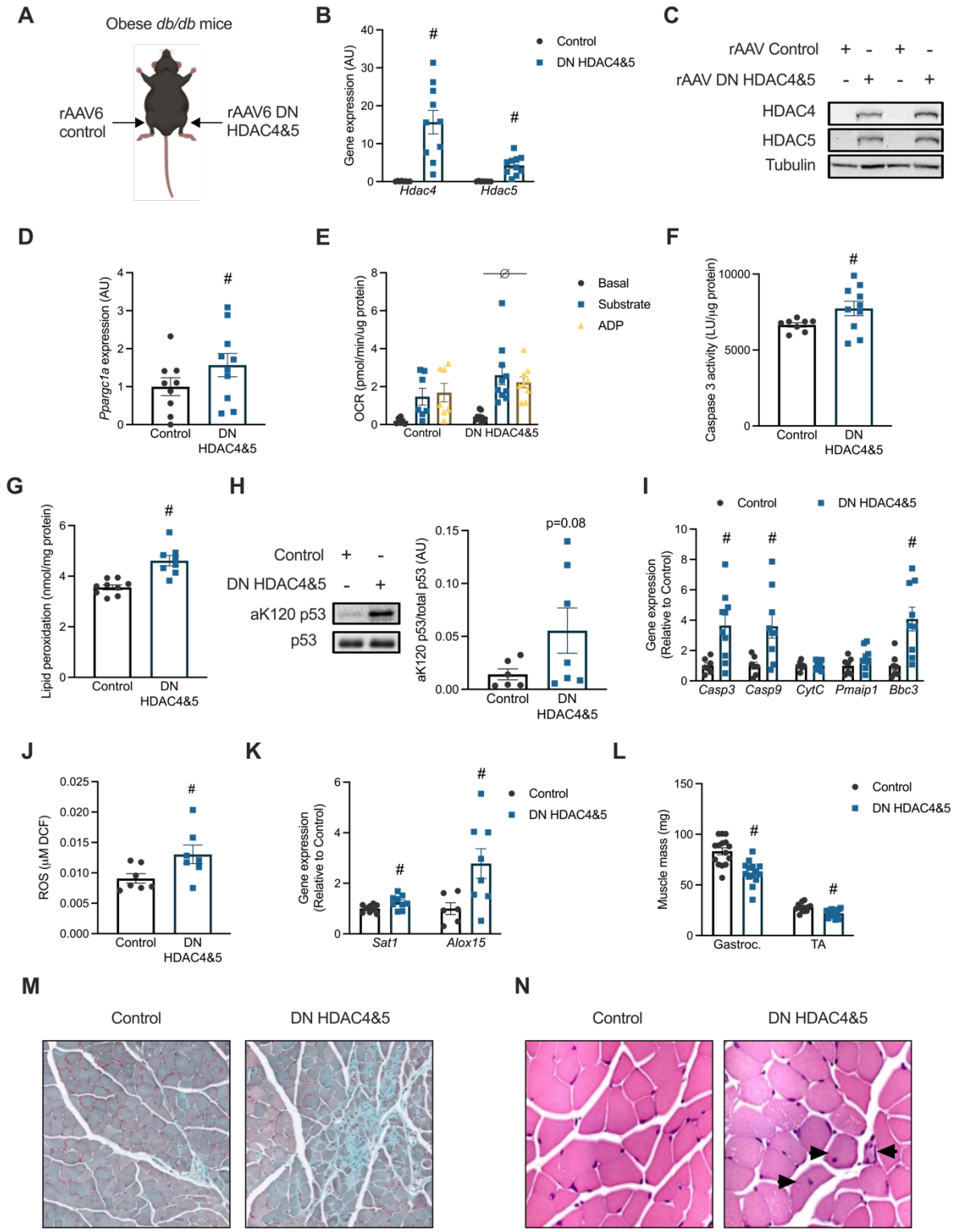
A
Obese db/db mice
rAAV6 control
rAAV6 DN HDAC4&5
B
Gene expression (AU)
Control
DN HDAC4&5
Hdac4
Hdac5
C
rAAV Control
rAAV DN HDAC4&5
HDAC4
HDAC5
Tubulin
D
Ppargc1a expression (AU)
Control
DN HDAC4&5
E
OCR (pmol/min/ug protein)
Basal
Substrate
ADP
F
Caspase 3 activity (LU/µg protein)
G
Lipid peroxidation (nmol/mg protein)
H
aK120 p53
p53
aK120 p53/total p53 (AU)
p=0.08
I
Gene expression (Relative to Control)
Casp3
Casp9
CytC
Pmaip1
Bbc3
J
ROS (µM DCF)
K
Sat1
Alox15
L
Muscle mass (mg)
Gastroc.
TA
M
N